Self-induced thermal effects and modal competition in continuous-wave optical parametric oscillators

R. O. Moore, G. Biondini, and W. L. Kath

Engineering Sciences and Applied Mathematics, McCormick School of Engineering and Applied Science, Northwestern University, 2145 North Sheridan Road, Evanston, Illinois 60208

Received May 2, 2001; revised manuscript received September 13, 2001

We present a model of quasi-phase-matched continuous-wave optical parametric oscillators that accounts for self-induced heating of the photorefractive crystal and modal interaction through pump depletion. The model allows the temperature and therefore the refractive index of the nonlinear medium to vary in the radial and longitudinal dimensions as a result of local absorption of the optical power. We consider the effect of this nonuniform index on single-mode and multimode operation. For a single signal–idler pair we observe thermal lensing, bulk tuning, and modal distortion. For multiple pairs of signal and idler we demonstrate and discuss other phenomena, including spatially dependent modal competition. © 2002 Optical Society of America

OCIS codes: 190.4870, 190.4970, 190.2620, 190.4420.

1. INTRODUCTION

Optical parametric oscillators (OPOs) are regarded as promising sources of high-power, coherent, narrow-linewidth infrared light, which makes them appealing for applications such as spectroscopy, laser radar, remote sensing, and infrared countermeasures[1,2] in either pulsed or continuous-wave (cw) form. Numerous investigations of the properties of OPOs were made in the late 1960s and early 1970s,[3] but at that time the usefulness of OPOs was limited by the availability of coherent and high-power pump lasers and by difficulties associated with the manufacture of crystals with uniform physical properties and high damage thresholds. These limitations were recently overcome by improvements in manufacturing techniques and by the development of periodically poled materials that permit simple access to the largest element of the quadratic polarization tensor through quasi phase matching.[4] OPOs based on engineered crystals such as periodically poled lithium niobate (PPLN) therefore have considerably lower threshold powers than the earlier versions, and they permit noncritical phase matching over a large range of signal and idler wavelengths while offering a host of new *in situ* tuning mechanisms.[5,6] [This broad tunability is generally available only in singly resonant oscillators (SROs), which do not impose constraints simultaneously on the pump and the idler frequencies through cavity resonance.] The advances in OPO threshold reduction, power output, and tunability have fueled a surge of renewed interest in OPOs, particularly those based on PPLN. The first successful bulk PPLN-based OPOs were produced in 1995[4,7,8] with oscillation thresholds well below the damage threshold of the crystals, and in the following year the high gain of PPLN was used to construct a tunable, cw SRO with a threshold of a few watts.[9] Several experimental papers on PPLN-based OPOs in a variety of operating regimes and in different cavity types have since appeared.

Because the oscillation threshold depends on the peak power, whereas thermal effects generally depend on the average power, cw SROs are particularly susceptible to the detrimental effects of heating. In lithium niobate SROs, thermal effects are typically attributable either to idler absorption (owing to the relatively high linear absorption coefficient for wavelengths in the far infrared[10]) or to signal absorption (owing to the often high intracavity signal power[11,12]). Experimental studies have made reference to thermal lensing and detuning as factors that limit the output efficiency and quality of OPOs,[11] and a number of numerical studies to facilitate a better understanding of these phenomena have been performed.[12–15] Most of these numerical investigations either neglected longitudinal variation of the crystal temperature or used a steady-state temperature profile, neglecting transient interaction between the field evolution and the temperature evolution. Arisholm conducted a limited study of the transient temperature evolution[16]; his principal comment was that such a study, which includes thermally induced nonuniformities in the refractive index, should also include multiple longitudinal modes so the way in which they compete can be observed.

Thermal effects have also been suggested as the cause of coupling to higher spatial modes in OPO output,[17] particularly when the field hops across a large range of longitudinal modes because of the presence of an intracavity optical element, e.g., an etalon with a large free spectral range. The resultant hopping of the output radial mode can be problematic in the fixed-aperture detectors used in spectroscopic applications, as the power through the ap-

erture can fluctuate erratically with time and with tuned signal wavelength. It is therefore important to investigate this behavior to be able to understand its cause and to mitigate its effects.

In this paper we present a numerical study of temperature-dependent phenomena in singly resonant OPOs. To analyze the effect of heating on SRO operation and output, we follow the spatial and temporal dependence of the temperature of the PPLN crystal. In particular, we consider the effect of a self-induced temperature profile on a single signal–idler pair and on multiple signal–idler pairs. We analyze the consequences for efficiency and spatial structure and for competition between the resonant pairs for pump power. To improve the speed of the computations significantly, we limit the simulations to radially symmetric profiles and devise a numerical advancement method that takes advantage of quasi-steady thermal deposition rates. We observe that the interaction between the process of field mixing and the temperature evolution can produce long-time mode hopping and that multiple signal–idler pairs can coexist for extended periods of time, typically with different transverse modal structures. This demonstration shows that even modest increases in temperature can lead to significant deformation of output transverse modes and that longitudinal mode hopping caused by spatially nonuniform heating can be accompanied by coupling to higher spatial modes with radically different energy distributions. These effects are similar to those seen in recent experiments performed with cw OPOs for spectroscopic applications.[17]

The following sections are organized as follows: In Section 2 we discuss the physical OPO model and its derivation, and in Section 3 we present the numerical method used to solve the partial differential equations. In Section 4 we outline the physical parameter range that we considered and the results that we obtained from the numerical study. The final section includes our conclusions based on these results.

2. MODEL

The basis of our analytical model is a linear, singly resonant cavity with a bulk PPLN crystal positioned between concave mirrors, as depicted in Fig. 1. The cavity is composed of two concave mirrors in free space that contain a PPLN crystal of large enough cross section relative to typical spot sizes that the edge effects can be neglected. We disregard reflections from the crystal faces, e.g., by assuming the presence of an antireflection coating or a slight wedge in the faces.[18] The wavelength dependence of the mirror reflectivities is included in the model, as is the effect of their curvature on the field phases. Because of their low reflectivity at either mirror, the pump and the idler fields are propagated only in the forward direction and then discarded, whereas the signal field inside the cavity is tracked throughout its forward and backward propagation. During their forward propagation, the pump, signal, and idler fields are taken to have negligible temporal walk-off, given their short interaction length. The crystal is assumed to be perfectly poled and to have mostly uniform physical properties. The only exception is the refractive index, which is taken to depend on local temperature. This temperature is, of course, driven by the deposit of optical energy from the interacting fields. The assumption of quasi-phase-matched operation enters into a scaled value of the nonlinear coefficient and an effective value of the phase mismatch that accounts for the leading order poling wavelength.[19]

Fig. 1. SRO with linear cavity. Dashed arrow indicates the option of seeded or unseeded signal.

In our consideration of multiple signal–idler pairs we take the modes to be separated by a frequency interval that is much larger than that which corresponds to the free spectral range of the cavity. This frequency separation could be accomplished by use of an intracavity element, such as a Fabry–Perot filter; we do not, however, explicitly model the behavior of the intracavity element. Our reason for using a wide frequency interval between modes is threefold: (i) we are interested primarily in longitudinal modes with significantly different spatial distributions of optical energy, which typically have a large separation in frequency; (ii) such large frequency separations could result from intracavity filters intended to narrow the OPO linewidth; and (iii) a comprehensive consideration of neighboring cavity modes must involve the relatively large number that are above or near threshold, and this number is currently computationally intractable at the level of detail of our simulations.

We derive the system of equations used in the model from Maxwell's equations in the usual fashion by decomposing the field and polarization into components at the pump, signal, and idler frequencies. The envelopes are assumed to vary slowly with respect to the rapid phase oscillations, and the nonlinearity is assumed to be instantaneous. Both of these assumptions are reasonable for cw parametric amplification in a photorefractive crystal. The fields are taken to be copolarized along the optic axis of the crystal and to be propagating in a direction orthogonal to this axis, as is appropriate for noncritically phase-matched operation. This orientation eliminates spatial walk-off and implies that the polarization vector is parallel to the electric field. The resultant equations for parametric amplification include diffraction, nonlinear mixing, and loss to absorption. In addition, we take into account the leading order influence of a spatially varying refractive index to capture the effect of a rise in temperature owing to absorption of field energy.

The derivation proceeds as follows: Maxwell's equations, under the assumptions of no intrinsic magnetic polarization, no free carriers, and a divergence-free field, yield the nonlinear wave equation

$$\nabla^2\mathbf{E} - \frac{\partial^2}{\partial t^2}\left(\frac{1}{c^2}\mathbf{E} + \mu_0\mathbf{P}\right) = 0. \tag{1}$$

A forward-propagating wave ansatz is used for the complex field, with the assumption that the mutual interaction of counterpropagating wave components is averaged out because of the fast relative phase oscillation:

$$\mathbf{E} = \sum_{j=p,s,i} \frac{1}{2}\{\exp[i(k_j z - \omega_j t)]E_j(\mathbf{r}, t) + \text{c.c.}\}\hat{c}, \quad (2)$$

where $\hat{c}$ is a unit vector parallel to the optic axis of the OPO crystal. A similar ansatz is made for the polarization vector:

$$\mathbf{P} = \sum_{j=p,s,i} \frac{1}{2}[\exp(-i\omega_j t)P_j(\mathbf{r}, t) + \text{c.c.}]\hat{c}, \quad (3)$$

where P_j are defined by the combinations of linear and quadratic terms in the field expansion that satisfy conservation of energy, as dictated by $\omega_p = \omega_s + \omega_i$:

$$P_p = \epsilon_0\{\chi^{(1)}(T, \omega_p)E_p \exp(ik_p z) + \chi^{(2)}(\omega_p, \omega_s, \omega_i)E_s E_i \exp[i(k_s + k_i)z]\}, \quad (4a)$$

$$P_s = \epsilon_0\{\chi^{(1)}(T, \omega_s)E_s \exp(ik_s z) + \chi^{(2)}(\omega_s, \omega_p, -\omega_i)E_p E_i^* \exp[i(k_p - k_i)z]\}, \quad (4b)$$

$$P_i = \epsilon_0\{\chi^{(1)}(T, \omega_i)E_i \exp(ik_i z) + \chi^{(2)}(\omega_i, \omega_p, -\omega_s)E_p E_s^* \exp[i(k_p - k_s)z]\}. \quad (4c)$$

Note that we have introduced the dependence of linear susceptibility $\chi^{(1)}$ on temperature T. Equations (4) are substituted back into Eq. (1), and terms of equal phase are collected to yield separate partial differential equations for pump, signal, and idler. Under the slowly varying envelope approximation ($|k_j E_j| \gg |\partial E_j/\partial z|$; Ref. 20) and the condition of a long nonlinear length (relative to the length scale of a carrier oscillation), the leading order simply produces a definition for the propagation constant:

$$k_j = \frac{n(T_{\text{amb}}, \omega_j)\omega_j}{c} \equiv \frac{n_j \omega_j}{c}, \quad (5)$$

where $n^2(T, \omega) = 1 + \Re[\chi^{(1)}(T, \omega)]$ and T_{amb} is the ambient (i.e., cold) temperature of the crystal's environment. We then write $n^2(T, \omega) \approx n_j^2 + 2n_j \Delta n_j$, where

$$\Delta n_j = \Delta n(\mathbf{r}, \omega_j) \equiv n[T(\mathbf{r}), \omega_j] - n_j. \quad (6)$$

Note that in Eq. (6) we retain variations of the index only with temperature and not with frequency. This is done because we consider the group-velocity mismatch to be small over the length of the crystal and we therefore neglect it. The index perturbation is pushed to the next-to-leading order, along with diffraction, loss (which arises from the imaginary part of the linear susceptibility), and nonlinear mixing through the quadratic terms. The slowly varying envelope approximation then yields

$$\frac{\partial E_p}{\partial z} - \frac{i}{2k_p}\nabla_\perp^2 E_p - \frac{2\pi i}{\lambda_p}\Delta n_p E_p + \frac{\alpha_p}{2}E_p = \frac{2\pi i}{n_p \lambda_p} d_{\text{eff}} E_s E_i \exp(-i\Delta k z), \quad (7a)$$

$$\frac{\partial E_s}{\partial z} - \frac{i}{2k_s}\nabla_\perp^2 E_s - \frac{2\pi i}{\lambda_s}\Delta n_s E_s + \frac{\alpha_s}{2}E_s = \frac{2\pi i}{n_s \lambda_s} d_{\text{eff}} E_p E_i^* \exp(i\Delta k z), \quad (7b)$$

$$\frac{\partial E_i}{\partial z} - \frac{i}{2k_i}\nabla_\perp^2 E_i - \frac{2\pi i}{\lambda_i}\Delta n_i E_i + \frac{\alpha_i}{2}E_i = \frac{2\pi i}{n_i \lambda_i} d_{\text{eff}} E_p E_s^* \exp(i\Delta k z), \quad (7c)$$

where $\nabla_\perp^2$ is the diffraction operator in the transverse plane, λ_j are the free-space wavelengths of the three fields, $\alpha_j \equiv (\omega_j/n_j c)\Im[\chi^{(1)}(T_{\text{amb}}, \omega_j)]$ are the loss coefficients, and d_{eff} is the effective quadratic coefficient of the medium, taken to be $d_{\text{eff}} = (2/\pi)d_{33} \equiv (1/\pi)\chi_{33}^{(2)}$ in a quasi-phase-matched material such as PPLN.[4] The nonlinear susceptibility tensor $\chi^{(2)}$ is taken to be spatially uniform, and its dependence on frequency is neglected. The phase-mismatch term that appears in Eqs. (7) is given by $\Delta k = k_p - k_s - k_i - 2\pi/\Lambda$, where Λ is the spatial period of the PPLN domains. The wavelengths are related by conservation of energy in the parametric process, so $1/\lambda_p = 1/\lambda_s + 1/\lambda_i$ (or, equivalently, $\omega_p = \omega_s + \omega_i$).

To study the behavior of multimode systems, we augment these equations by introducing an additional signal–idler pair. The additional pair does not interact directly with the original pair[21]; rather, it interacts with the pump in a manner similar to the interaction between the pump and the first pair, and its governing equations are therefore identical. Obviously, the frequencies of the second signal–idler pair must still satisfy the condition imposed by conservation of energy: $\omega_p = \omega_{s_2} + \omega_{i_2}$. The additional equations are

$$\frac{\partial E_{s_2}}{\partial z} - \frac{i}{2k_{s_2}}\nabla_\perp^2 E_{s_2} - \frac{2\pi i}{\lambda_{s_2}}\Delta n_{s_2} E_{s_2} + \frac{\alpha_{s_2}}{2}E_{s_2} = \frac{2\pi i}{n_{s_2}\lambda_{s_2}} d_{\text{eff}} E_p E_{i_2}^* \exp(i\Delta k_2 z), \quad (8a)$$

$$\frac{\partial E_{i_2}}{\partial z} - \frac{i}{2k_{i_2}}\nabla_\perp^2 E_{i_2} - \frac{2\pi i}{\lambda_{i_2}}\Delta n_{i_2} E_{i_2} + \frac{\alpha_{i_2}}{2}E_{i_2} = \frac{2\pi i}{n_{i_2}\lambda_{i_2}} d_{\text{eff}} E_p E_{s_2}^* \exp(i\Delta k_2 z). \quad (8b)$$

The additional nonlinear depletion of the pump must also be taken into account, changing the pump's evolution equation (7a) into

$$\frac{\partial E_p}{\partial z} - \frac{i}{2k_p}\nabla_\perp^2 E_p - \frac{2\pi i}{\lambda_p}\Delta n_p E_p + \frac{\alpha_p}{2}E_p = \frac{2\pi i}{n_p \lambda_p} d_{\text{eff}}[E_{s_1} E_{i_1} \exp(-i\Delta k_1 z) + E_{s_2} E_{i_2} \exp(-i\Delta k_2 z)], \quad (9)$$

where we now use subscripts 1 and 2 to distinguish between the two signal–idler pairs. We should emphasize that this additional signal–idler pair is not necessarily meant to represent neighboring cavity modes, with a corresponding spacing of a few gigahertz (i.e., a few picometers), in an effort to approximate the effect of a broad linewidth. Rather, it represents a spacing of a few maxima of an intracavity element such as a Fabry–Perot

filter, with a corresponding free spectral range of a few hundred terahertz (i.e., a few nanometers).

We assume that the heating of the crystal beyond the ambient temperature is due only to the absorption of power from the three fields, and we limit its effect to a nonuniform change in the refractive index. For instance, we do not allow for external temperature control, and we do not take into account the linear expansion of the crystal. The evolution equation for the temperature is the forced three-dimensional heat equation:

$$\frac{\partial T}{\partial t} = D_h \nabla^2 T + \frac{\epsilon_0 c}{2\rho c_p}(\alpha_{s_1} n_{s_1} |E_{s_1}|^2 + \alpha_{i_1} n_{i_1} |E_{i_1}|^2 + \alpha_{s_2} n_{s_2} |E_{s_2}|^2 + \alpha_{i_2} n_{i_2} |E_{i_2}|^2 + \alpha_p n_p |E_p|^2), \tag{10}$$

where t is time, D_h is the crystal diffusivity, ρ is the crystal density, and c_p is the crystal's constant-pressure heat capacity. The parameters ϵ_0 and c represent the permittivity constant and the speed of light, respectively. The temperature is assumed to tend to its ambient value T_{amb} far from the propagation axis, and on either face of the crystal the boundary condition is taken to be Newtonian cooling, given by

$$\kappa \frac{\partial T}{\partial z} = -h(T - T_{\mathrm{amb}}), \tag{11}$$

where κ is the thermal conductivity and the emissivity h includes the effects of convection and radiation.

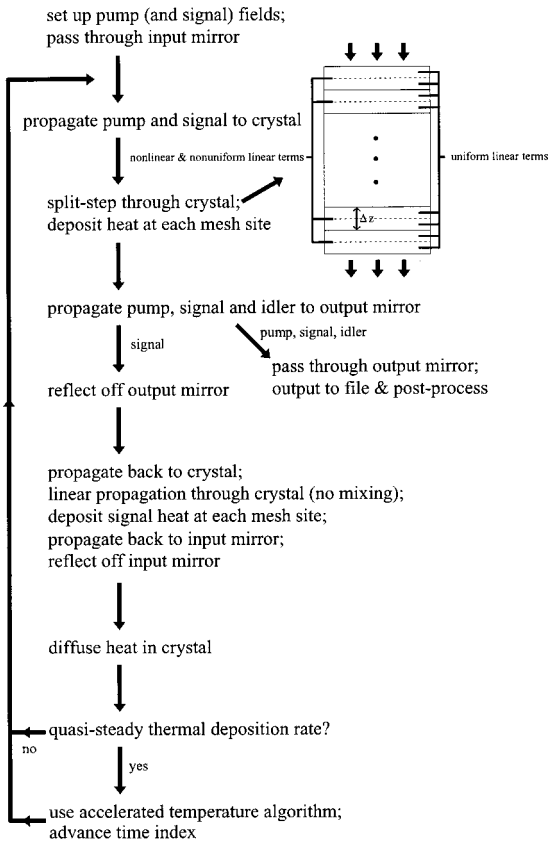

Fig. 2. Flow chart and schematic of the field evolution and temperature deposit–diffusion algorithm.

3. NUMERICAL METHOD

The basic structure of our numerical scheme is illustrated in Fig. 2. The system of equations (7)–(9) is integrated numerically by use of an algorithm that is similar in spirit to that used by Smith *et al.*[22] and by Arisholm[23] and that builds on the beam propagation method.[24] The idea is to integrate a single slice of the optical fields through the crystal by use of a transform routine in combination with an efficient and accurate time stepper, such as the Runge–Kutta algorithm, in a split-step scheme. When the fields reach the end of the cavity, the signals are reflected off the end mirror and propagated back to the input mirror. A new pump slice is then injected, and, if the OPO is seeded, new input signal slices are added to the existing signals. The process is then repeated. Arbitrary temporal resolution can be achieved by addition of more slices within a round-trip time of the fields; however, this method is not currently capable of accommodating significant group-velocity mismatch or dispersion.

Our numerical algorithm takes advantage of the radial symmetry of the noncritically phase-matched OPO by neglecting the azimuthal dependence of the fields, thereby decreasing the dimensionality of the problem to 1 + 1 dimensions. This has an obvious advantage over a full (2 + 1)-dimensional approach in that it speeds up the integrations considerably. We use Hankel transforms to integrate the spatially homogeneous linear part of the evolution equations. The zeroth-order Bessel function basis is also more efficient than a Fourier basis at representing the transverse cavity modes, enabling us to use fewer numerical modes. The numerical Hankel transform that we use is the quasi-discrete Hankel transform;[25] for a discussion and comparison with other Hankel transform routines see Ref. 26.

The signal field is seeded by injection of an initial energy equal to a single photon in a Gaussian spatial profile. As was pointed out by Smith *et al.*,[27] this model is not appropriate for capturing accurately the broadband behavior of an unseeded OPO; however, we are interested in observing its behavior after it has reached the slow-transient operating regime with moderate or high power levels. The low-amplitude seeding is intended simply to start the OPO off in a naturally selected mode, and the macroscopic field equations are appropriate once the signal and idler amplitudes have reached a sufficient magnitude.[21] No interpretation is made of the field evolution before that point is reached.

Diffusion of the temperature profile within the crystal occurs on a scale of milliseconds, compared with the nanosecond-scale round-trip time of the fields in the OPO cavity. The two processes can therefore effectively be treated independently of each other on each pass through the crystal, with the local deposit of heat being calculated immediately on integration of the field equations and the diffusion operator applied to the crystal temperature profile after each full round trip is completed by the field slices. Again, a schematic of this procedure is given in Fig. 2. Integration of the temperature profile is performed with a Crank–Nicholson scheme on the Hankel-transformed diffusion equation. To observe the model's

behavior over time scales long enough for thermal diffusion to play a role, we have developed an acceleration algorithm to skip unnecessary optical field integrations and thereby reduce the computational run time. We make use of the fact that, for a constant crystal temperature profile, the optical fields typically reach a steady state within tens of nanoseconds. By accelerating the advancement of the temperature profile in a controlled way, we skip some of the intermediate field states, postulating that the mean behavior will qualitatively be the same. The algorithm works as follows: On each pass of the field slices, we monitor the spatially dependent thermal deposition rate in the crystal that is due to absorption plus diffusion. When the change in this rate drops below a certain threshold for a few passes, signaling that the field amplitudes through the crystal are relatively stationary, we speed up the rate of temperature change throughout the crystal by multiplying the nonuniform thermal deposition seen over the previous round trip by an integer factor. This factor is chosen to be inversely proportional to the derivative of mean thermal deposition rate calculated from the previous two round trips, and its magnitude is limited to allow the algorithm to approach a steady state. This technique allows us to investigate the field and temperature evolution over long time scales of the order of the crystal's characteristic thermal diffusion time while it sacrifices information about the optical field only during periods of relatively slow temperature change. We have verified that the temperature profiles produced by this technique are relatively robust to the acceleration parameters used. The field output is also qualitatively the same, although specific times of noteworthy field changes (e.g., mode hops) vary somewhat, depending on the acceleration parameters.

4. RESULTS

Using our numerical model, we, first, study the effect of heating on single-mode operation and, second, investigate the behavior of a competing pair of signal and idler fields under the influence of self-heating. The parameters used for our runs are based on the experiments of Bosenberg *et al.*,[9] who used a 104-mm linear cavity containing a 50-mm PPLN crystal inside mirrors with 50-mm radii of curvature. The ambient temperature was approximately 175 °C, and the wavelength-dependent parameters are listed in Table 1. The input pump energy was taken to be 13 W, and the signal and idler were generated from noise of random phase. All the input fields were set to achieve a beam waist ($1/e^2$ radius) of 97 μm at the center of the crystal. Values of $\kappa = 5.6$ W/mK and $\rho = 4644$ kg/m^3 were used for the conductivity and the density, respectively, of lithium niobate.[10,28] Given the dearth in the literature of reliable reference values for h, a value for the organic crystal that was found in Ref. 15, i.e., $h = 25$ W/m^{2}K, was used.

The numerical runs were performed at a resolution of 100 longitudinal grid points and 128 radial points. Both numbers were varied to ensure proper convergence. The domain radius was set at 1.4 mm to ensure negligible field amplitudes at the exterior boundary.

A. Single Signal–Idler Pair

1. OPO Characteristics

We begin by noting how the output characteristics of the OPO in its simplest operational mode of a single signal–idler pair are affected by the presence of a self-induced temperature profile. Figures 3 and 4 illustrate this configuration run out to steady state and the resultant temperature profile, respectively. Comparison with runs without thermal effects (e.g., Fig. 9 below) shows that the inclusion of heating considerably delays the achievement of a steady state (this is essentially a confirmation of the existence of two disparate time scales in the equations) and that the final output spatial profile of the signal is significantly different when the crystal is allowed to heat nonuniformly.

We used the temperature profile illustrated in Fig. 4 to compare the OPO tuning and efficiency characteristics with and without self-induced heating present in the model. Figure 5 demonstrates the well-known phenomenon of temperature tuning, as the center wavelength of the OPO tuning curve is increased with increased mean temperature. The acceptance bandwidth of the OPO also increases in the presence of a self-induced temperature profile, which appears to be due to the fact that the spatially nonuniform refractive index facilitates coupling between the initially Gaussian field profiles and higher-order transverse modes of the OPO. The tuning curves of these higher-order modes are shifted from the tuning curve of a simple Gaussian, leading to a broadened tuning curve for the collection of possible transverse modes. These effects are discussed below in the context of the interaction between competing modes. Figure 6 compares the plots of output signal power and input pump power, with and without the nonuniform temperature field present. As was already demonstrated in Fig. 5, the efficiency is decreased significantly on average at the originally well-tuned wavelength of 1.57 μm, which also increases the threshold of the simulations performed with the temperature field present. Comparison of Fig. 6 with Fig. 2 of Ref. 9 shows reasonable quantitative agreement with respect to the idler power, but the signal powers given by the simulations are considerably higher than those seen in experiment. That this is so is likely due to the fact that we have disregarded signal absorption in

Table 1. Wavelength-Dependent OPO Parameters

λ (nm)	Unperturbed Refractive Index	Absorption Coefficient (cm^{-1})	Input Reflectance	Output Reflectance
1064 (pump)	2.16	0	0.02	0.14
1570 (signal)	2.14	0	0.997	0.995
3301 (idler)	2.09	0.2	0.03	0.11

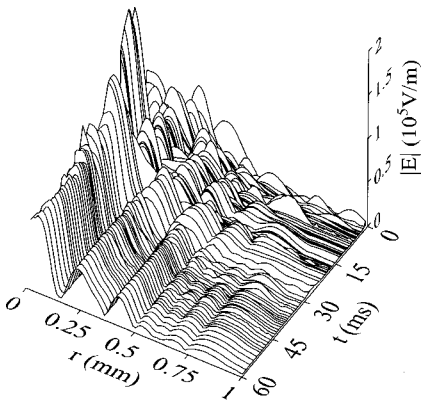

Fig. 3. Signal field run to steady state, with self-induced heating.

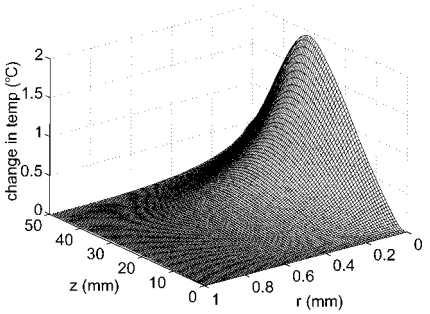

Fig. 4. Steady-state temperature in crystal with a single signal–idler pair.

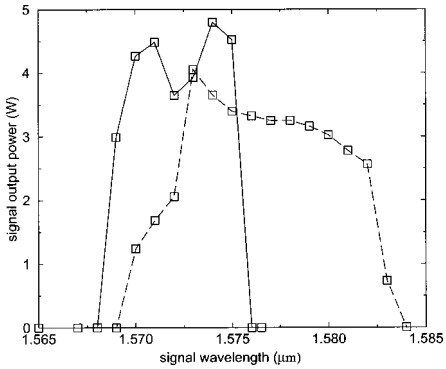

Fig. 5. Tuning curve of signal output power versus signal wavelength, without (solid curve) and with (dashed curve) a self-induced nonuniform temperature profile. Input pump power, 13 W.

these simulations, preferring to focus on the case of high absorption at the idler wavelength.

2. Self-Induced Heating and Thermal Lensing

The temperature profiles generated through self-heating during our numerical runs depend on the relative sizes of the absorption coefficients used at the signal and idler wavelengths and on the relative power levels of each inside the crystal. The absorption coefficient at the idler wavelength in the far-infrared region is significantly higher in lithium niobate than the absorption coefficient at the pump and signal wavelengths.[12] Figure 7 shows a typical temperature profile generated during a run with two simultaneously present signal wavelengths, at 1.570 and 1.569 μm. In this situation, idler absorption is the dominant heating mechanism, which is apparent from Fig. 7 by the lack of heating at the input face of the crystal. Also discernible from Fig. 7 is the saturation of the nonlinear mixing process significantly before the end of the crystal, implying that the choice of crystal length may not be optimal in these operating conditions.

Using this temperature field, we propagated initially Gaussian pump and (seeded) signal fields independently through the crystal to observe how their transverse pro-

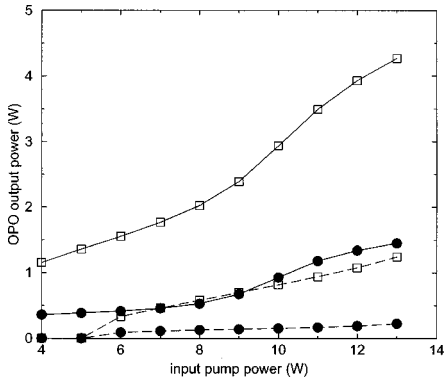

Fig. 6. Output signal (squares) and idler (filled circles) power versus input pump power, without (solid curves) and with (dashed curves) a self-induced nonuniform temperature profile. Signal wavelength, 1.57 μm.

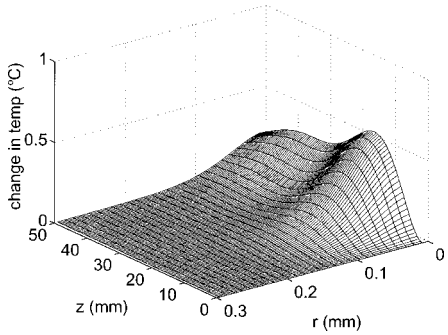

Fig. 7. Longitudinal (z) and radial (r) variation in the crystal temperature.

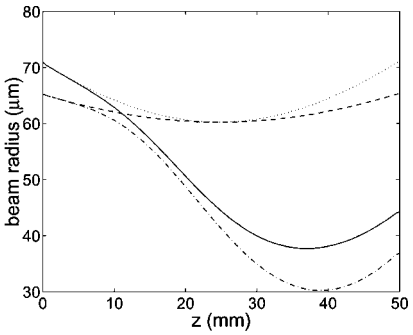

Fig. 8. Thermal lensing experienced by a signal and a pump passing through a crystal with a nonuniform temperature profile. Shown are the beam radii for the signal with a uniform temperature profile (dotted curve) and with a nonuniform temperature profile (solid curve) and for the pump with a uniform temperature profile (dashed curve) and with a nonuniform temperature profile (dashed–dotted curve). Nonlinear mixing was turned off in these runs.

Table 2. Output Powers of OPO with Uniform Crystal Temperatures Adjusted to Effect Perfect Quasi Phase Matching, Adjusted to 0.5 °C above Perfect Phase Matching, and with a Nonuniform Crystal Temperature Generated from Previous Runs with a Maximum Slightly Less Than 0.5 °C[a]

Crystal Temperature (°C)	Signal Power	Idler Power	Pump Power	Heating Power
175[b]	0.925	0.323	0.670	0.30
175.5 ($\Delta k \neq 0$)	0.789	0.277	0.944	0.23
$175 < T(r,z) < 175.5$	0.388	0.142	1.75	0.15

[a] Input pump power, 3 W. All field powers are in watts.
[b] Perfect quasi phase matching.

files were affected by the nonuniform index in the absence of any nonlinear mixing. Figure 8 shows the value of the signal and pump beam widths as the beams travel through the medium with nonuniform index and through a uniform medium for comparison. Obviously, the signal beam diffracts more than the pump beam because of the signal's larger wavelength. The beam widths are significantly altered by the presence of the nonuniform temperature field. Both beams are focused, so their intensities are higher during much of their interaction, suggesting that, for operation only moderately above threshold, the index perturbation might assist conversion efficiency by increasing the local intensities of the two beams where they overlap. The runs performed to verify this hypothesis, however, show a significantly reduced efficiency when the index perturbation is present, even compared with runs with a spatially uniform refractive index (i.e., uniform but detuned) equal to the maximum of the spatially varying index. The relatively low efficiency of the runs with a nonuniformly perturbed refractive index implies that local detuning and distortion of the field profiles from the nonuniform refractive index destroy any potential improvement in conversion efficiency caused by the thermal lensing, as clearly also holds for higher conversion levels. Table 2 lists the effects of this temperature profile on conversion efficiencies for various power inputs. Also given in Table 2 is the calculated power dedicated to heating the crystal, after power lost through reflections from the end mirrors is considered.

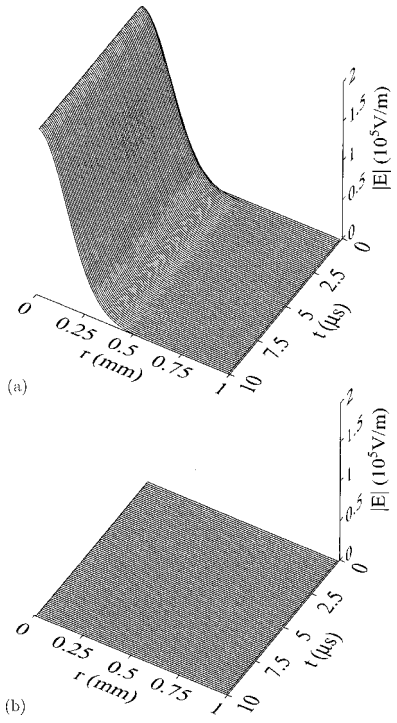

Fig. 9. Two signal beams, at 1.570 μm (top) and 1.576 μm (bottom), with no heating effects included. Note that, in the absence of temperature effects, the beams reach steady state very quickly.

B. Two Signal–Idler Pairs

1. Thermally Induced Shift in the Gain Curve

The primary and better-understood effect[19] of a rise in the crystal temperature is to shift the phase-matched tuning curve. Such a shift can lead to the growth of longitudinal modes that will remain below threshold in the absence of self-induced heating. This effect, introduced in Subsection 4.A.1, is demonstrated in Figs. 9 and 10, which show two simultaneous signal–idler pairs operating at 1.570/3.301 and 1.576/3.275 μm, respectively, with and without the presence of self-induced heating. The first signal–idler pair is chosen to lie at the center of the quasi-phase-matched gain spectrum in the absence of heating. In the first case, i.e., without heating, the first signal–idler pair is well above threshold, whereas the second pair is below threshold. Consequently, only the first signal is present. In the second case, however, the average shift in index caused by the heating is sufficient to deflect the gain curve to the point where the second signal–idler pair is above threshold. The two pairs are then seen to exist simultaneously in the cavity, although it is reasonable to expect that the crystal temperature might eventually reach a point at which the original signal–idler pair is no longer within the acceptance bandwidth, which would return the OPO to single-mode operation at the second signal–idler pair. Figure 11 shows the temperature profile at the end of the run in Fig. 10. Note that the temperature is not yet at a steady state, as is evident from Fig. 10. We ran multiple-pair simulations to steady state, but they are not included here because of space constraints.

It is clear that a rise in crystal temperature causes a net decrease in gain at the originally well-tuned signal wavelength as well as distortions of the spatial beam profile owing to the dependence of the mixing efficiency on local phase variations. Another effect illustrated in Fig. 10 is the effect of this shift in the gain peak on the signal beam profile. It has already been suggested[29] that, in detuned OPO operation, the gain experienced by certain off-axis modes (or modes with nonzero radial wave number) can be higher than the gain experienced by on-axis

modes. We believe that the jump in spatial mode that occurs after approximately 0.14 ms in the 1.570-μm field in Fig. 10 is a manifestation of the same phenomenon, in which the thermal detuning leads to a higher spatial mode that experiences more gain than the Gaussian mode that built up in the cold cavity. As the crystal heats further, this deformation of the spatial mode of the original signal frequency gives way to growth of a new, thermally tuned signal frequency. The spatial profile of the second signal has a significant portion of its energy away from the propagation axis, suppressing the off-center component of the original signal's spatial profile.

2. Modal Competition

Finally, we explored the behavior of our numerical OPO model over longer time scales, for which thermal diffusion is relevant. To avoid unreasonably long run times while preserving accuracy, we adopted the method of advancing the temperature profile described in Section 3. This

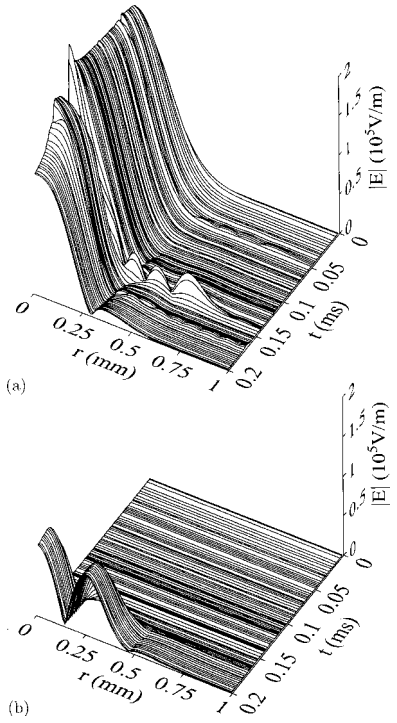

Fig. 10. Two signal beams, at 1.570 μm (top) and 1.576 μm (bottom), with heating effects included.

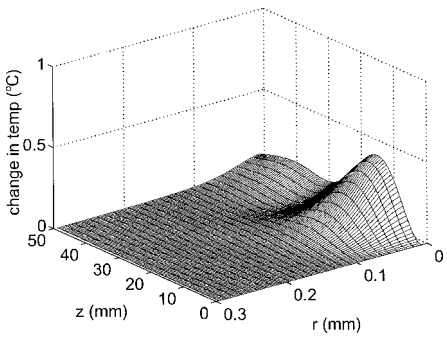

Fig. 11. Transient temperature profile (at $t = 0.2$ ms) accompanying Fig. 10.

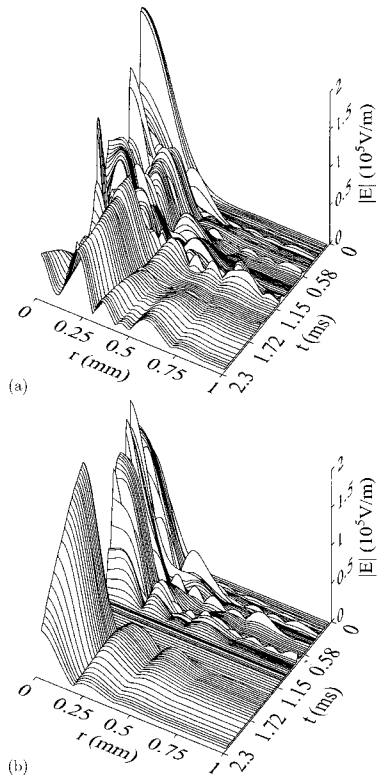

Fig. 12. Two signals separated by the free spectral range of an etalon (wavelengths, 1.570 and 1.569 μm). The first signal is perfectly phase matched at zero initial temperature buildup.

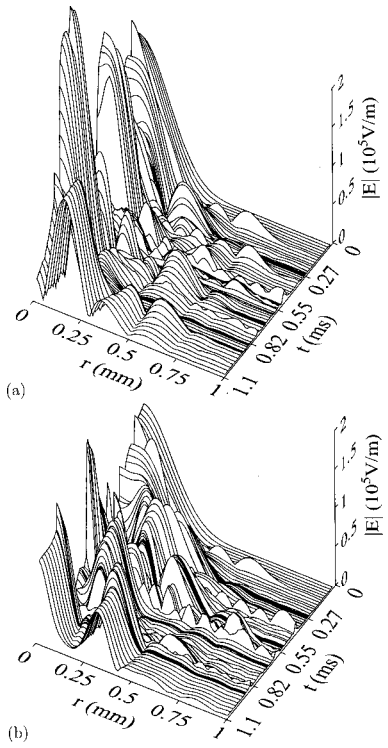

Fig. 13. Two signals separated by the free spectral range of an etalon (wavelengths, 1.570 and 1.571 μm). The first signal is perfectly phase matched at zero initial temperature buildup.

technique allowed us to observe runs of millisecond duration and beyond, which is ~6 orders of magnitude longer than the physical round-trip time of the cavity. Over these longer durations, we observed a number of complex spatiotemporal phenomena, including periods of nearly stationary evolution separated by rapid readjustments and the near extinction and regrowth of one of the signal–idler pairs. Figures 12 and 13 demonstrate a typical run involving two longitudinal mode (signal–idler) pairs separated by the free spectral range of an etalon, equal to 1 nm. For the first pair of signals the second signal's wavelength is smaller than the phase-matched wavelength at uniform ambient temperature. An increase in temperature therefore drives the phase-matching curve even further from the second signal, which is evidenced in the figure by the relatively low output power of the second signal toward the end of the run. In the second run, the second signal wavelength is slightly greater than the phase-matched wavelength, so the temperature increase drives the phase-matching curve closer to this value. It is clear from the figure, however, that the temperature has not been allowed to build to the point where the first wavelength is far enough out of the phase-matching curve to suffer extinction. The redistribution of power in this figure suggests that the temperature deviation at the center of the crystal has tuned the phase-matching curve to the second frequency but that this curve now varies radially, in keeping with the radial variation of the temperature profile.

These results show that nonuniform heating of the crystal through absorption of optical power leads not only to coupling between neighboring cavity (or filter) modes but also to irregular spatial distributions of optical power in both modes at the OPO output. Such spatial irregularities can give rise to serious problems in calibrating the single-frequency power output of fixed-aperture narrow-bandwidth devices such as spectrometers. The alternating regions of near extinction and significant conversion in Fig. 12 also suggest the possible existence of bistable operating regimes in which the OPO undergoes a cyclical behavior that involves heating, detuning, extinction, retuning, and heating again. Clearly, these fluctuations are undesirable in laser applications that depend on stable single-mode output power and beam quality.

5. CONCLUSIONS

We have developed a numerical model with which to investigate self-induced thermal effects in single-mode and multimode operation of a cw, noncritically phase-matched optical parametric oscillator. The model is fully time dependent and is scalable from runs of nanosecond duration (optical field evolution scale) to runs of millisecond duration (thermal evolution scale). Furthermore, the choice of a noncritically phase-matched configuration allows us to decrease the run time considerably by using Hankel transforms rather than two-dimensional Fourier transforms.

Simulation of single-mode operation shows clear evidence of thermal lensing that results from the spatial nonuniformity of the refractive index caused by a local increase in temperature throughout the crystal. This increase also has the overall effect of tuning the longitudinal mode at the center of the crystal's gain profile. It is not generally true that the thermal lensing and resultant enhancement of signal and pump overlap can be exploited to improve conversion; rather, this uncontrolled waveguide serves to disrupt the phase-matching process in such a way that the OPO's efficiency deteriorates as the temperature profile grows.

In simulating operation with multiple signal–idler pairs we have demonstrated that at least two such nondegenerate pairs can be stable simultaneously in the cavity, as has already been suggested in analytical studies.[30] The competition between these pairs is affected not only by the average thermal tuning of the crystal but also by the spatial structure imparted to these pairs by the nonuniform index perturbations. The average tuning effect is essentially a mean shift in phase mismatch Δk, but it has been shown that this shift in itself can lead to detuned longitudinal modes with higher-order transverse structures.[29] The nonuniform Δk complicates matters further by giving rise to spatial coupling (through depletion of the pump) between the competing modes, which changes significantly as the crystal increases in temperature.

This temporal variation of the spatial structure of the modes is demonstrated in our simulation on times scales appropriate for significant thermal evolution. During these longer runs we see the crystal's temperature reach a quasi-steady state, while the optical fields continue to undergo a drift in their transverse profiles. This result suggests the possibility of bistable operation in which thermal detuning decreases the efficiency of the mixing process, causing a drop in heat deposited through absorption. We did not directly observe such bistability, however.

Each of the phenomena discussed here has serious implications for devices that rely on stably single-mode infrared beams with constant spatial power distributions. A better understanding of these effects is therefore critically important for improvement of the reliability of these devices, particularly in environments outside the laboratory. Given the intractable nature of their governing equations and the complexity of the coupling between the electric fields and the crystal temperature, numerical methods such as the one presented here are becoming increasingly more important as we attempt to find ways to avoid or mitigate the detrimental influence of self-induced temperature increases on OPO efficiency, stability, and output beam quality.

ACKNOWLEDGMENTS

We thank Peter Powers, Ken Schepler, and Scott Bisson for many valuable discussions.

This study was supported in part by U.S. Air Force Office of Scientific Research award F49620-99-1-0016. R.O. Moore (e-mail: rmoore@northwestern.edu) acknowledges the financial support of the Natural Sciences and Engineering Research Council of Canada.

REFERENCES

1. B. A. Richman, K. W. Aniolek, T. J. Kulp, and S. E. Bisson, "Continuously tunable, single-longitudinal-mode, pulsed mid-infrared optical parametric oscillator based on periodically poled lithium niobate," J. Opt. Soc. Am. B **17**, 1233–1239 (2000).
2. F. K. Hopkins, "Military laser applications: providing focus to nonlinear optics R & D," Opt. Photon. News, February, 1998, pp. 32–38.
3. Y. X. Fan and R. L. Byer, "Progress in optical parametric oscillators," in *New Lasers for Analytical and Industrial Chemistry*, A. Bernhardt, ed., Proc. SPIE **461**, 27–32 (1984).
4. L. E. Myers, R. C. Eckardt, M. M. Fejer, R. L. Byer, W. R. Bosenberg, and J. W. Pierce, "Quasi-phase-matched optical parametric oscillators in bulk periodically poled $LiNbO_3$," J. Opt. Soc. Am. B **12**, 2102–2116 (1995).
5. N. O'Brien, M. Missey, P. Powers, V. Dominic, and K. L. Schepler, "Electro-optic spectral tuning in a continuous-wave, asymmetric-duty-cycle, periodically poled $LiNbO_3$ optical parametric oscillator," Opt. Lett. **24**, 1750–1752 (1999).
6. P. E. Powers, T. J. Kulp, and S. E. Bisson, "Continuous tuning of a continuous-wave periodically poled lithium niobate optical parametric oscillator by use of a fan-out grating design," Opt. Lett. **23**, 159–161 (1998).
7. L. E. Myers, G. D. Miller, R. C. Eckardt, M. M. Fejer, and R. L. Byer, "Quasi-phase-matched 1.064-μm-pumped optical parametric oscillator in bulk periodically poled $LiNbO_3$," Opt. Lett. **20**, 52–54 (1995).
8. V. Pruneri, J. Webjorn, P. S. Russell, and D. C. Hanna, "532 nm pumped optical parametric oscillator in bulk periodically poled lithium-niobate," Appl. Phys. Lett. **67**, 2126–2128 (1995).
9. W. R. Bosenberg, A. Drobshoff, J. I. Alexander, L. E. Myers, and R. L. Byer, "Continuous-wave singly resonant optical parametric oscillator based on periodically poled $LiNbO_3$," Opt. Lett. **21**, 713–715 (1996).
10. V. G. Dmitriev, G. G. Gurzadyan, and D. N. Nikogosyan, *Handbook of Nonlinear Optical Crystals*, Vol. 64 of Springer Series in Optical Sciences (Springer-Verlag, Berlin, 1997).
11. W. R. Bosenberg, J. I. Alexander, L. E. Myers, and R. W. Wallace, "2.5-W, continuous-wave, 629-nm solid-state laser source," Opt. Lett. **23**, 207–209 (1998).
12. D. D. Lowenthal, "CW periodically poled $LiNbO_3$ optical parametric oscillator model with strong idler absorption," IEEE J. Quantum Electron. **34**, 1356–1366 (1998).
13. M. A. Dreger and J. K. McIver, "Second-harmonic generation in a nonlinear, anisotropic medium with diffraction and depletion," J. Opt. Soc. Am. B **7**, 776–784 (1990).
14. S. Severini, C. Sibilia, and M. Bertolotti, "Transverse effects in a parametric down-conversion process in three dimensions," J. Opt. Soc. Am. B **17**, 580–585 (2000).
15. P. Kerkoc, S. Horinouchi, K. Sasaki, Y. Nagae, and D. Pugh, "Thermal effects on second-harmonic generation in biaxial molecular crystals," J. Opt. Soc. Am. B **16**, 1686–1691 (1999).
16. G. Arisholm, "Advanced numerical simulation models for second-order nonlinear interactions," in *Laser Optics '98: Fundamental Problems of Laser Optics*, N. N. Rosanov, ed., Proc. SPIE **3685**, 86–97 (1999).
17. S. E. Bisson, Sandia National Laboratories, 7011 East Ave., MS 9051, Livermore, Calif. (personal communication, 2000).
18. L. E. Myers, R. C. Eckardt, M. M. Fejer, R. L. Byer, and W. R. Bosenberg, "Progress in quasi-phasematched optical parametric oscillators using periodically poled $LiNbO_3$," in *Nonlinear Frequency Generation and Conversion*, **2700**, 216–226 (1996).
19. L. E. Myers and W. R. Bosenberg, "Periodically poled lithium niobate and quasi-phase-matched optical parametric oscillators," IEEE J. Quantum Electron. **33**, 1663–1672 (1997).
20. G. P. Agrawal, *Nonlinear Fiber Optics*, 2nd ed. (Academic, San Diego, Calif., 1995).
21. A. Fix and R. Wallenstein, "Spectral properties of pulsed nanosecond optical parametric oscillators: experimental investigation and numerical analysis," J. Opt. Soc. Am. B **13**, 2484–2497 (1996).
22. A. V. Smith, W. J. Alford, T. D. Raymond, and M. S. Bowers, "Comparison of a numerical-model with measured performance of a seeded, nanosecond KTP optical parametric oscillator," J. Opt. Soc. Am. B **12**, 2253–2267 (1995).
23. G. Arisholm, "General numerical methods for simulating second-order nonlinear interactions in birefringent media," J. Opt. Soc. Am. B **14**, 2543–2549 (1997).
24. M. D. Feit and J. J. A. Fleck, "Light propagation in graded-index optical fibers," Appl. Opt. **17**, 3990–3998 (1978).
25. L. Yu, M. C. Huang, M. Z. Chen, W. Z. Chen, W. D. Huang, and Z. Z. Zhu, "Quasi-discrete Hankel transform," Opt. Lett. **23**, 409–411 (1998).
26. R. O. Moore, "A study of optical devices with parametric gain," Ph.D. dissertation (Northwestern University, Evanston, Ill., 2001).
27. A. V. Smith, R. J. Gehr, and M. S. Bowers, "Numerical models of broad-bandwidth nanosecond optical parametric oscillators," J. Opt. Soc. Am. B **16**, 609–619 (1999).
28. Almaz Optics, Inc., "Lithium niobate, $LiNbO_3$," http://www.almazoptics.com/homepage/LiNbO3.htm.
29. S. Longhi, "Spatio-temporal instabilities and threshold condition in a broad-area optical parametric oscillator," Opt. Commun. **153**, 90–94 (1998).
30. C. Fabre, P. F. Cohadon, and C. Schwob, "CW optical parametric oscillators: single mode operation and frequency tuning properties," Quantum Semiclassic. Opt. **9**, 165–172 (1997).